Electronic Supplementary Material (ESI) for Journal of Materials Chemistry A.

Nanoflower-like MoS_2 anchored on electrospun carbon nanofibers-interpenetrated reduced graphene oxide as microbial fuel cells anode achieving high power density

Yuanfeng Liu, [abc] Tingli Ren, [abc] Zijing Su, [abc] Congju Li [*abc]

a. School of Energy and Environmental Engineering, University of Science and Technology Beijing, Beijing 100083, China;
b. Beijing Key Laboratory of Resource-oriented Treatment of Industrial pollutants, Beijing 100083, China;
c. Energy Conservation and Environmental Protection Engineering Research Center in Universities of Beijing, Beijing 100083, China.

* Corresponding author: congjuli@126.com

Calculation methods

Equation S1:

(1) The specific capacitance (C_p) values were calculated by the following equation:

$$C_p = \frac{\int_{V1}^{V2} i\,dv}{2As(V2 - V1)} \quad (1)$$

Where V_1 represented the initial potential, V_2 was the final potential, i was the instantaneous current, A was the anode surface area (4.5 cm^{-2}), and s represented the scan rate (V s^{-1}).

Equation S2:

(2) The COD removal efficiency in a batch mode were calculated as follows:

$$COD(\%) = \frac{(COD_{in} - COD_{out})}{COD_{in}} \times 100\% \quad (2)$$

Where COD_{in} *and* COD_{out} represented the inlet COD content and outlet COD content (mg L^{-1}), respectively.

Equation S3:

(3) The calculation formula of coulomb efficiency (CE) was as follows:

$$CE(\%) = \frac{M\int_{0}^{t} Idt}{FnV_{anode}\Delta COD} \quad (3)$$

Where *M* was the relative molecular weight of oxygen (32 g mol^{-1}); I was output current; t was the working time in a batch. *F* was the Faraday constant (96485 C mol^{-1}); *n* was the number of electrons transferred by oxidizing 1 mol organic substance with oxygen as standard (4 mol^{-} •mol^{-1}); V_{anodic} was the anode chamber volume (0.118 L); ΔCOD was removal content of the organic substance (mg L^{-1}) in one batch.

Table S1. The composition of the anolyte.

Samples	Components	Contents (L^{-1})	Purity	Source
Acetate- growth medium	NaAc	0.5 g	⩾98%	Sigma-Aldrich
	NH_4Cl	0.1 g	⩾99%	Macklin
	NaCl	0.5 g	⩾99%	Hopebio
	$NaHCO_3$	1 g	⩾99%	Sinopharm Chemical Reagent
	KH_2PO_4	0.53 g	⩾99%	Macklin
	Na_2HPO_4	3.3 g	⩾99%	Macklin
	HCl (25%)	10 mL	37%	Sinopharm Chemical Reagent
Trace element (2 mL)	$FeCl_3$ $4H_2O$	1.5 g	⩾98%	Sigma-Aldrich
	$ZnCl_2$	0.07 g	⩾99%	Sigma-Aldrich
	$MnCl_4$ $4H_2O$	0.1 g	⩾99%	Sigma-Aldrich
	$CoCl_2$ $6H_2O$	0.19 g	98%	Sigma-Aldrich

	$CuCl_2 \cdot 2H_2O$	2 mg	≥99%	Sigma-Aldrich
	$NiCl_2 \cdot 6H_2O$	0.02 g	≥98%	Sigma-Aldrich
	$NaMoO_4 \cdot H_2O$	0.04 g	≥99%	Sigma-Aldrich
vitamin solution (2 mL)	Biotin	20 mg	≥98%	Sigma-Aldrich
	Folic acid	20 mg	≥98%	Sigma-Aldrich
	Pyridoxine-HCl	100 mg	≥98%	Sigma-Aldrich
	Thiamine-HCl $\cdot 2H_2O$	50 mg	≥99%	Sigma-Aldrich
	Riboflavin	50 mg	100%	Santa cruz
	Nicotinic acid	50 mg	≥99%	Absin
	D-Ca-pantothenate	50 mg	≥98%	Sigma-Aldrich
	Vitamin B12	50 mg	≥99%	Cayman chemical
	Para-aminobenzoic acid	50 mg	≥99%	Sigma-Aldrich
	Thioctic acid	50 mg	≥98%	Raybiotech

Nicotinamide	50 mg	⩾98%	Absin
Lipoic acid	50 mg	⩾98%	Sigma-Aldrich
Hemin	50 mg	⩾90%	Sigma-Aldrich
1,2-Nnphthoquinone	50 mg	⩾99%	Sigma-Aldrich
Vitamin K2	50 mg	⩾98%	Cayman chemical

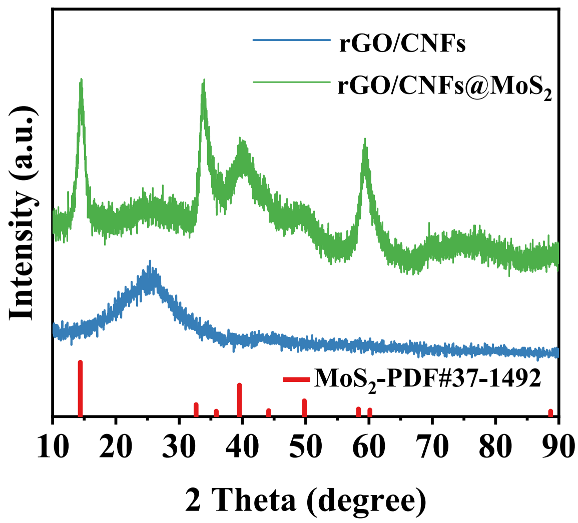

Fig. S1. XRD patterns of the prepared samples.

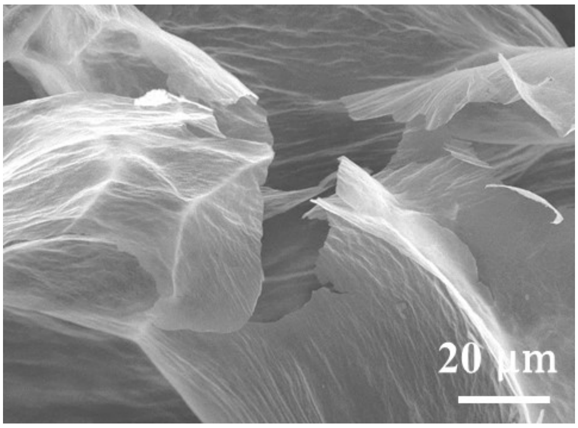

Fig. S2. SEM images of the rGO layers.

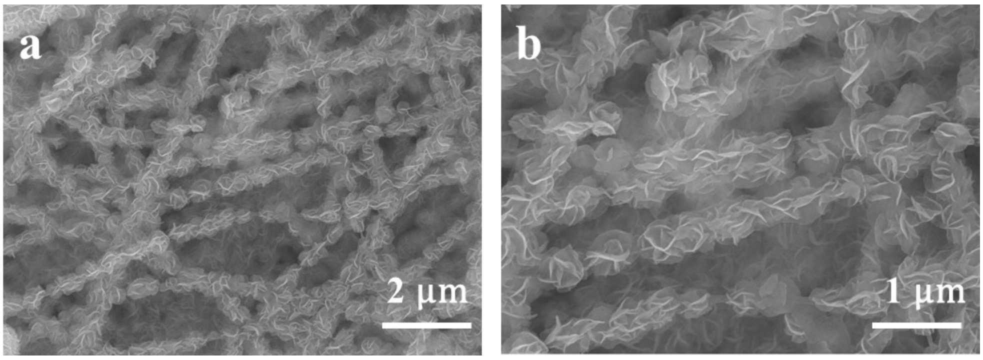

Fig. S3. SEM images of (a) the CNFs@MoS_2 electrocatalyst and (b) its magnification.

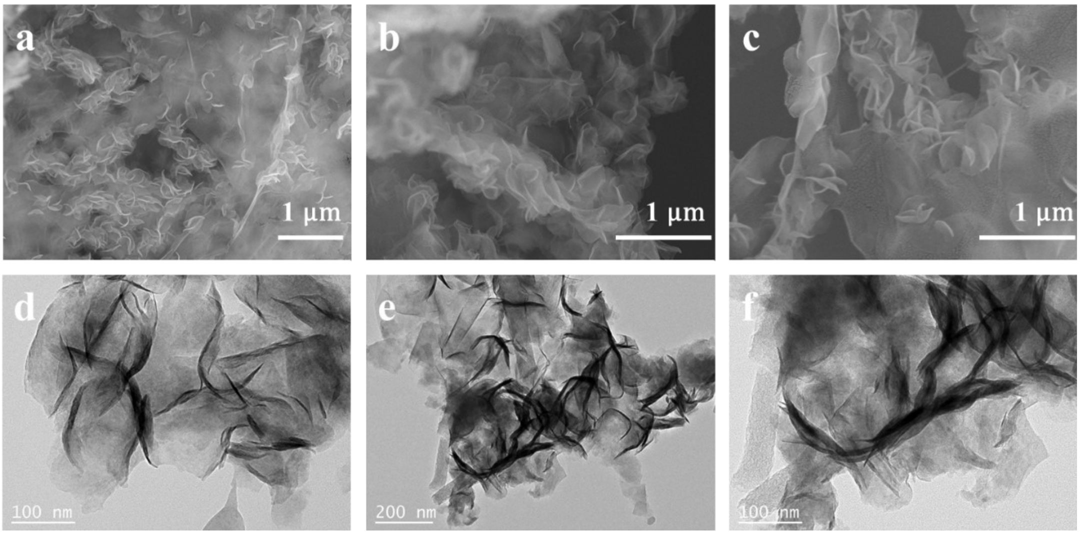

Fig. S4. SEM images of (a-c) the rGO/CNFs@MoS_2 electrocatalysts. TEM images of (d-f) the rGO/CNFs@MoS_2 electrocatalysts.

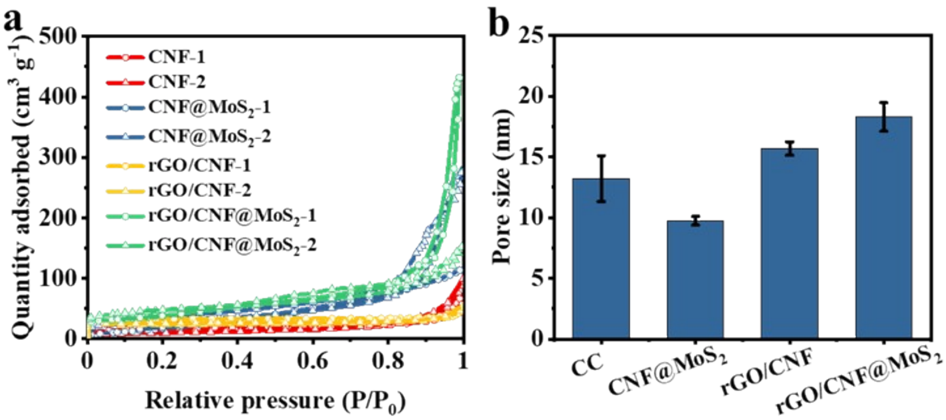

Fig. S5. (a) Nitrogen adsorption–desorption isotherms. (b) BJH pore size distributions.

Table S2. BET surface areas of different electrocatalysts.

Sample	**Surface area (cm^3 g^{-1})**	**Average value (cm^3 g^{-1})**	**Standard deviation**
CNF	49.8 36.2	43	6.7
CNF@MoS_2	72.4 80.4	76.4	4
rGO/CNF	129.8 103.4	116.6	13.2
rGO/CNF@MoS_2	142.8 158.8	150.5	7.7

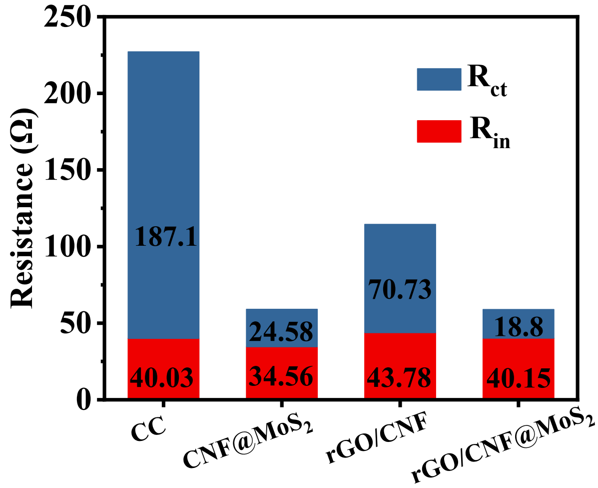

Fig. S6. The fitted resistance values of different anodes.

Table S3. Comparison of the MFC power density.

Anode	Inoculum	MFC type	Power density ($mW\ m^{-2}$)
HP-CNFs[1]	*S.Putrefaciens* CN32	Dual-chamber, 150 mL	1407.42
N-MWCNT/GA[2]	*Shewanella oneidensis*	Dual-chamber, 130 mL	2977.8
BL-PANI[3]	Wastewater	Dual-chamber, 28 mL	567.2
PPy/NFs/PET[4]	*Escherichia coli* (K12)	Dual-chamber, 500 mL	2420
FeCo/NCNTs@CF[5]	Wastewater	Dual-chamber, 100 mL	3040
NCP/LSC[6]	Anaerobic sludge	Single-chamber, 28 mL	1090
rGO/CNFs@MoS_2(This work)	Wastewater	Dual-chamber, 118 mL	3548

Note: HP-CNFs: Hierarchically porous carbon nanofibers; N-MWCNT/GA: Nitrogen-doped multiwalled carbon nanotube/graphene; PPy/NFs/PET: polypyrrole/poly(vinyl alcohol-co-poly-ethylene) nanofibers/poly(ethylene terephthalate); NCP/LSC: Nitrogen enriched PANI/loofah sponge carbon

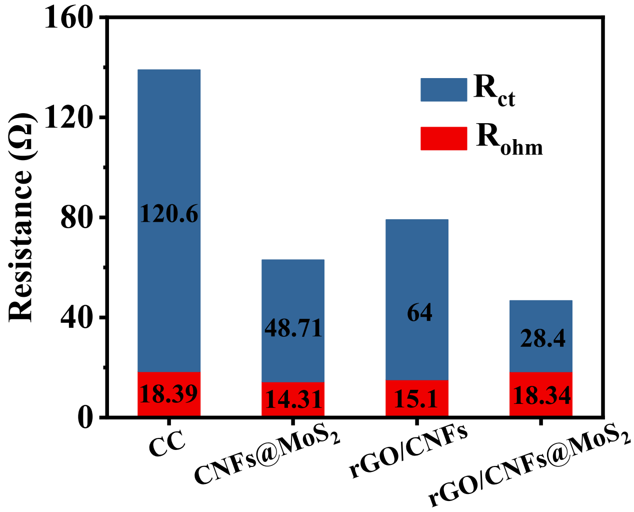

Fig. S7. The fitted resistance values of different bioanodes under turnovers.

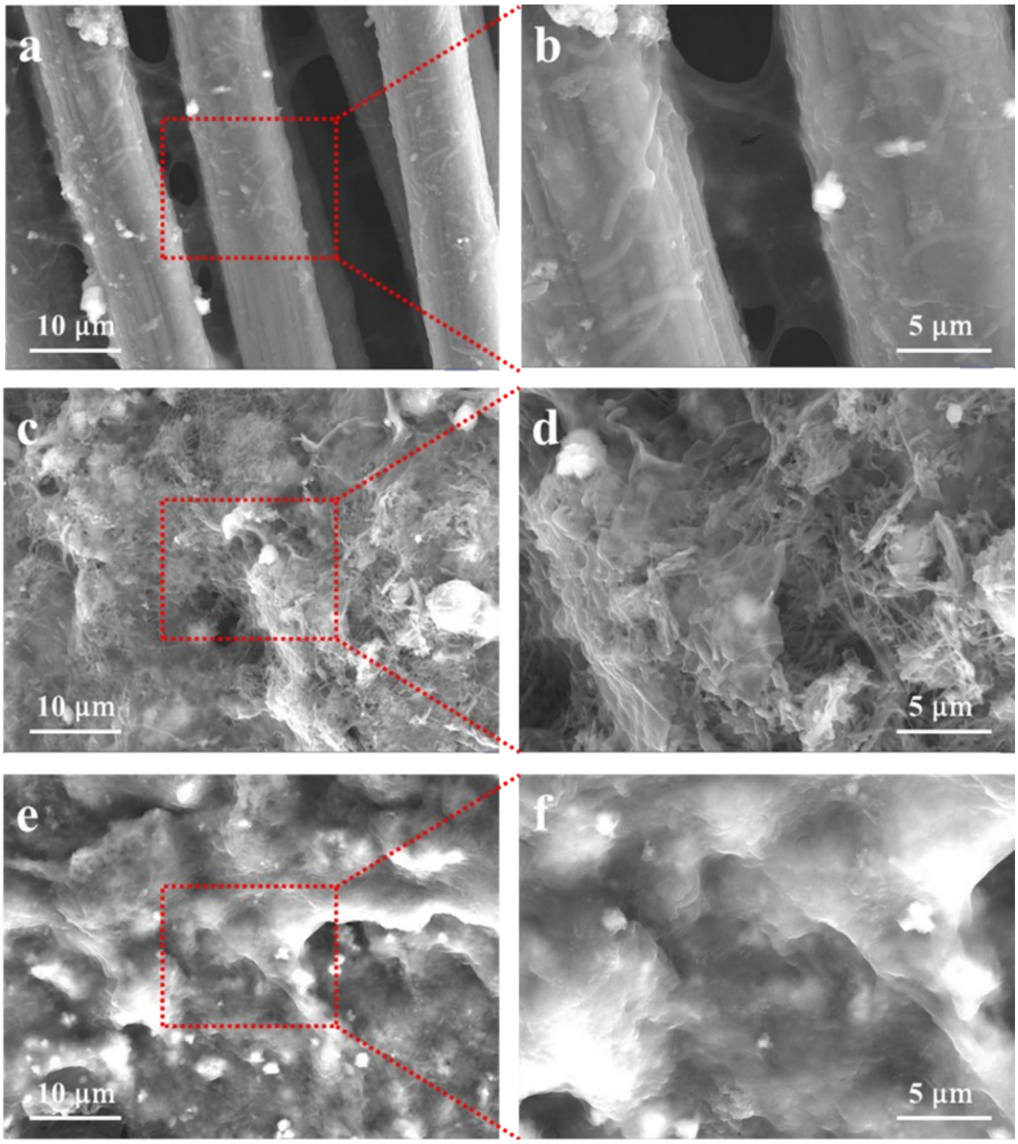

Fig. S8. SEM images of the biofilms grown on the (a, b) CC, (c, d) rGO/CNFs, and (e, f) rGO/CNFs@MoS_2

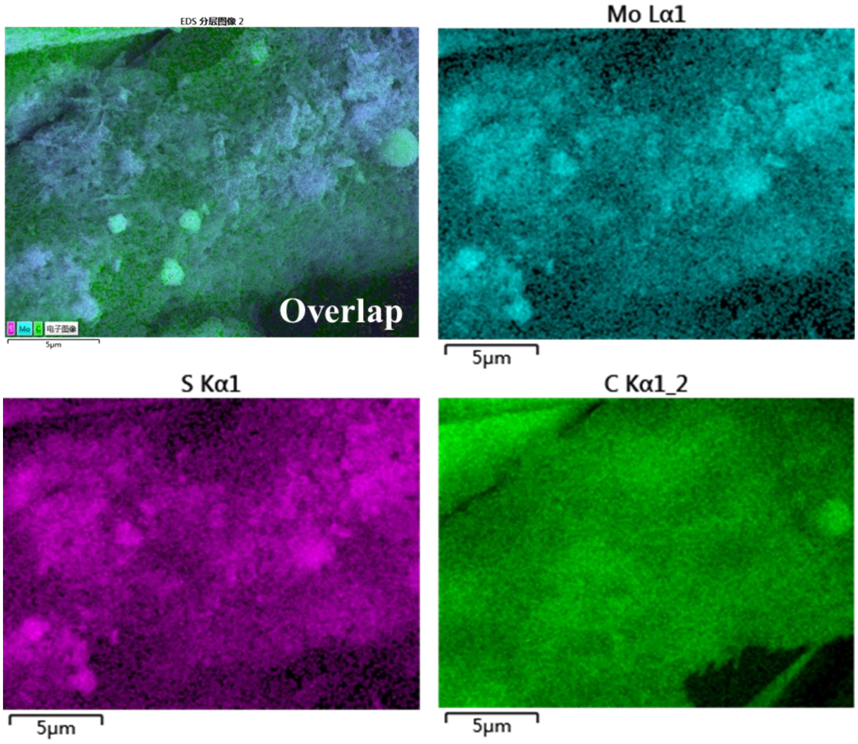

Fig. S9. EDX elemental maps of the biofilm with the CNF@MoS_2 electrocatalysts.

At the end of the experiment, we further performed the XPS analysis to examine the electronic structures of Mo and S elements in the biofilms. As shown in Fig. S10, the high-resolution Mo 3d XPS spectrum exhibited two spin-orbital doublet peaks at 229.4 eV and 232.6 eV, which can be assigned to Mo^{4+}. Additionally, a weak peak at the binding energy of 236 eV was related to Mo^{6+}, implying the presence of Mo^{4+} and Mo^{6+} in the biofilm. The existence of multiple valance states of the Mo element in the biofilms is conducive to mediating the interspecific electron transfer and information exchange process, thus improving the power generation of MFC.[7] The high-resolution S 2p XPS spectrum suggested the existence of divalent sulfide ions (S^{2-}) in the biofilms. Wang et al. [8]reported that elemental sulfur can serve as electron shuttles to mediate electron-shuttling during bacterial colonization. Based on the above analysis, the Mo and S species embedded in the biofilms were favorable for EET.

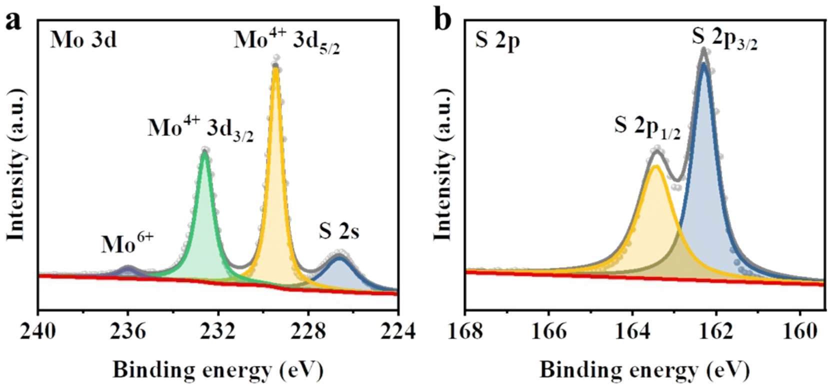

Fig. S10. The high-resolution XPS analysis of (a) Mo 3d, and (b) S 2p.

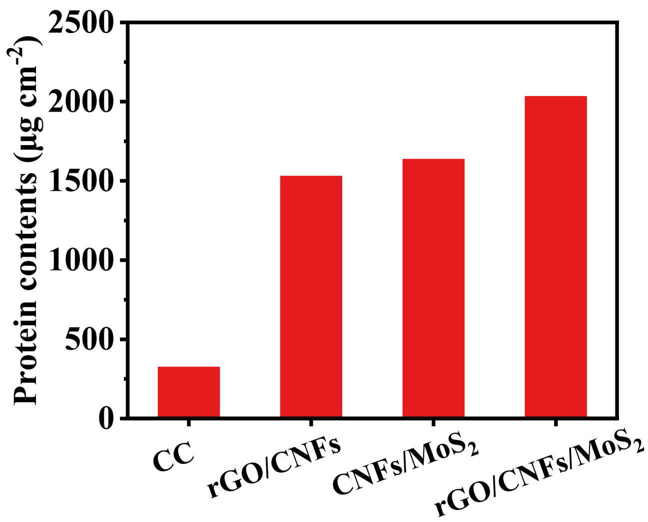

Fig. S11. The protein contents on different anodes.

Table S4. Diversity and abundance index of the microbial community on different anodes.

Samples	Shannon[a]	Simpson[b]	Coverage	ACE[c]	Chao[c]	OTUs	Sequence
CC	4.01	0.058	0.998	487.3	468.5	640	48144
CNFs@MoS_2	4.19	0.045	0.998	569.5	564.8	769	53161
rGO/CNFs	4.5	0.025	0.999	492.4	484.3	751	50731
rGO/CNFs@MoS_2	4.63	0.023	0.999	570.9	578.9	859	65150

[a] The diversity index of the microbial community. A higher value indicates more diversity.

[b] The evenness index of the microbial community. A higher value indicates more evenness.

[c] The abundance index of the microbial community. A higher value indicates more abundance.

Fig. S12 presented multiple sets of experimental data toward the current density, power density and polarization curves of MFC, demonstrating the negligible deviation among the different data. Thus, intermediate values of power density and current density are adopted in the manuscript for normal analysis.

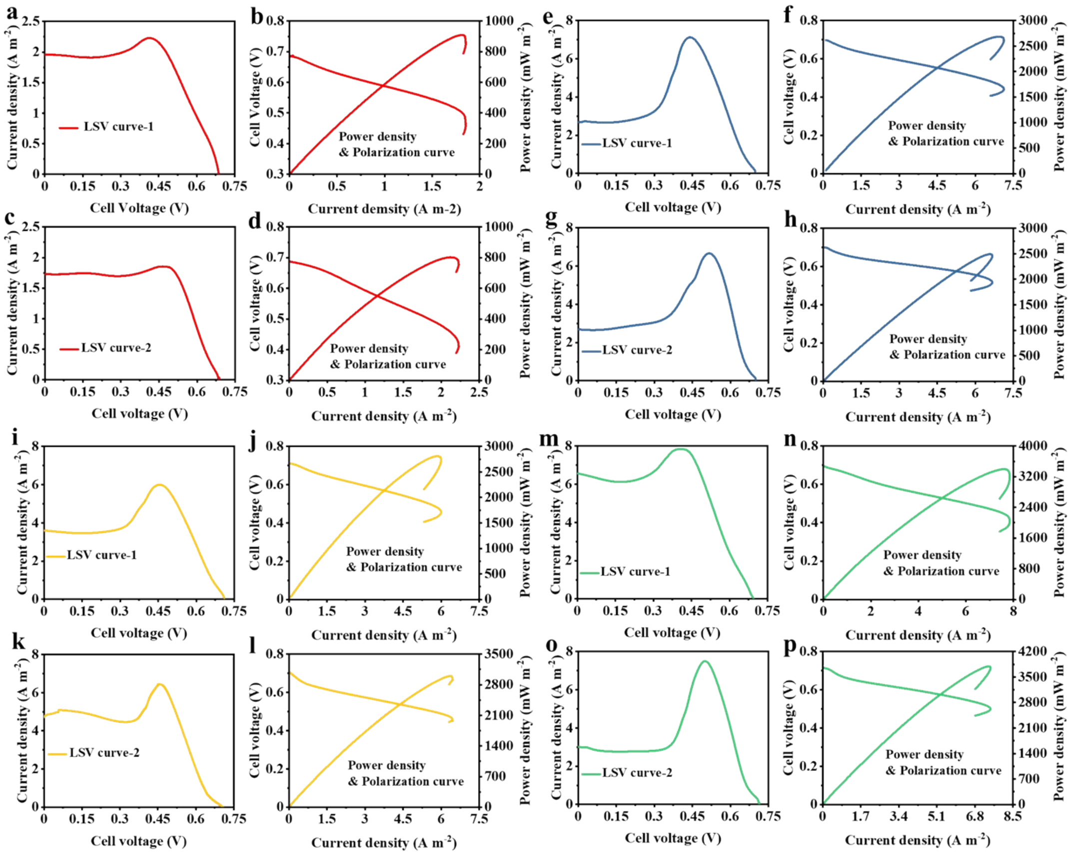

Fig. S12. MFC performance with different anodes (a-d) CC, (e-h) CNF@MoS_2, (i-k) rGO/CNF, (m-p) rGO/CNF@MoS_2

Table S5. Multiple sets of experimental data toward current density and power density.

Sample	Current density (A m^{-2})	Power density (mW m^{-2})	Mid-value
	2.23	909	
CC	2.61	805	805
	1.853	802	
	6.7	2493	
CNF@MoS_2	7.02	2560	2560
	7.12	2685	
	6.0	2809	
rGO/CNF	6.8	2992	2992
	6.4	2999	
	77.84	3396	
rGO/CNF@MoS_2	8.49	3584	3584
	7.49	3789	

Reference

1. S. Qian, X. Wu, Z. Shi, X. Li, X. Sun, Y. Ma, W. Sun, C. Guo and C. Li, *Nano Research*, 2022, **15**, 5089-5097.
2. S. Jin, Y. Feng, J. Jia, F. Zhao, Z. Wu, P. Long, F. Li, H. Yu, C. Yang and Q. Liu, *Energy & Environmental Materials*, 2022, **0**, 1-9.
3. W. Zhang, B. Xie, L. Yang, D. Liang, Y. Zhu and H. Liu, *Bioresource technology*, 2017, **233**, 291-295.
4. Y. Tao, Q. Liu, J. Chen, B. Wang, Y. Wang, K. Liu, M. Li, H. Jiang, Z. Lu and D. Wang, *Environmental science & technology*, 2016, **50**, 7889-7895.
5. Y. Wang, X. Cheng, K. Liu, X. Dai, J. Qi, Z. Ma, Y. Qiu and S. Liu, *ACS Applied Materials & Interfaces*, 2022, **14**, 35809-35821.
6. Y. Yuan, S. Zhou, Y. Liu and J. Tang, *Environmental science & technology*, 2013, **47**, 14525-14532.
7. X. Li, M. Hu, L. Zeng, J. Xiong, B. Tang, Z. Hu, L. Xing, Q. Huang and W. Li, *Biosensors and Bioelectronics*, 2019, **145**, 111727-111734.
8. R. Wang, M. Yan, H. Li, L. Zhang, B. Peng, J. Sun, D. Liu and S. Liu, *Advanced Materials*, 2018, **30**, 1800618-1800624.